

# Investigation of the Stability of the Poly(ethylene oxide)|LiNi<sub>1-x-y</sub>Co<sub>x</sub>Mn<sub>y</sub>O<sub>2</sub> Interface in Solid-State Batteries

Yuriy Yusim, Dirk F. Hunstock, Alexander Mayer, Dominic Bresser, Stefano Passerini, Jürgen Janek,\* and Anja Henss\*

While solid-state batteries (SSBs) comprising poly(ethylene oxide) (PEO) based electrolytes are successfully commercialized already for operation at elevated temperature, the selection of the cathode active material (CAM) has so far been limited to LiFePO<sub>4</sub>. When using high-voltage CAMs such as LiNi<sub>1-x-y</sub>Co<sub>x</sub>Mn<sub>y</sub>O<sub>2</sub> (NCM), the cells experience fast capacity fading – the cause of which is not consistently understood in literature. In this study, electrochemical impedance spectroscopy measurements in a three-electrode setup are applied to confirm that the NCM|PEO interface is indeed the Achilles' heel in PEO-based SSBs at high voltages. In this regard, the interfacial stability on the cathode side depends not only on the upper cut-off voltage, but also on the molecular weight of PEO, strongly affecting the cell performance. Scanning electron microscopy images of the cathodes after cycling suggest that at high voltages interfacial degradation leads to fragmentation of the polymer backbone and to a decrease in viscosity of the solid polymer electrolyte. Overall, the results help to understand the detrimental processes occurring in PEO-based SSBs in combination with high-voltage cathodes.

replacement of liquid electrolytes in LIBs by solid electrolytes (SEs) is, amongst others, motivated by the transition to high-capacity lithium-metal anodes, eventually leading to higher energy densities.<sup>[1]</sup> A large variety of SEs is currently investigated for the use in SSBs. Among all classes of SEs, that is, polymer-,<sup>[4]</sup> oxide-,<sup>[5]</sup> sulfide-<sup>[5]</sup> and halide-based<sup>[6]</sup> SEs, only solid polymer electrolytes (SPEs) based on poly(ethylene oxide) (PEO) with lithium bis(trifluoromethanesulfonyl)imide (LiTFSI) as conducting salt were successfully commercialized so far, which has been achieved by Blue Solutions (Bolloré Group) in 2012 using LiFePO<sub>4</sub> (LFP) as the cathode active material (CAM).<sup>[7]</sup> In addition to their moderate ionic conductivity at elevated temperatures ( $\approx 1 \text{ mS cm}^{-1}$  at 80 °C),<sup>[8]</sup> further advantages of PEO-based-SPEs for their application in SSBs include low cost and their malleable nature,

which allows good interfacial contact to the electrode active materials.<sup>[9]</sup>

Nevertheless, there are remaining challenges on the way to higher performance that must be addressed such as substituting the currently utilized low-voltage LFP by high-voltage CAMs such as (Ni-rich) LiNi<sub>1-x-y</sub>Co<sub>x</sub>Mn<sub>y</sub>O<sub>2</sub> (NCM) to achieve significantly higher energy densities, which results in rapid capacity fading. The processes occurring at the interface between the PEO-based

## 1. Introduction

Conventional state-of-the-art lithium-ion batteries (LIBs) with a liquid electrolyte are expected to reach their limits in terms of energy density.<sup>[1]</sup> However, the demand for batteries with even higher energy densities is increasing, mainly driven by the electrification of the transportation sector. To meet these demands, solid-state batteries (SSBs) have been regarded as one of the most promising next-generation energy storage devices.<sup>[1–3]</sup> The

Y. Yusim, D. F. Hunstock, J. Janek, A. Henss  
Institute of Physical Chemistry  
Justus Liebig University Giessen  
Heinrich-Buff-Ring 17, 35392 Giessen, Germany  
E-mail: juergen.janek@phys.chemie.uni-giessen.de;  
anja.henss@phys.chemie.uni-giessen.de

The ORCID identification number(s) for the author(s) of this article can be found under <https://doi.org/10.1002/admi.202300532>

© 2023 The Authors. Advanced Materials Interfaces published by Wiley-VCH GmbH. This is an open access article under the terms of the Creative Commons Attribution License, which permits use, distribution and reproduction in any medium, provided the original work is properly cited.

DOI: 10.1002/admi.202300532

Y. Yusim, D. F. Hunstock, J. Janek, A. Henss  
Center for Materials Research (ZfM/LaMa)  
Justus Liebig University Giessen  
Heinrich-Buff-Ring 16, 35392 Giessen, Germany  
A. Mayer, D. Bresser, S. Passerini  
Helmholtz Institute Ulm (HIU)  
Helmholtzstraße 11, 89081 Ulm, Germany  
A. Mayer, D. Bresser, S. Passerini  
Karlsruhe Institute of Technology (KIT)  
P.O. Box 3640, 76021 Karlsruhe, Germany  
S. Passerini  
Department of Chemistry  
Sapienza University of Rome  
P. Aldo Moro 5, Rome 00185, Italy

SE and NCM, however, are not yet well understood.<sup>[10]</sup> Different decomposition and failure mechanisms with high-voltage cathodes (NCM, LiCoO<sub>2</sub>) have been discussed in literature so far, which are briefly outlined in the following: Some studies found that oxidative electrolyte degradation is the main mechanism for battery failure, as concluded from a gradual thinning of the SPE layer and gas generation during cycling.<sup>[11,12]</sup> Other studies emphasized the crucial role of the conducting salt, suggesting the generation of bis(trifluoromethanesulfonyl)imide acid (HTFSI), which in turn chemically decomposes PEO.<sup>[12–14]</sup> Additional studies revealed that oxygen release from the CAMs also acts as further ingredient for PEO decomposition.<sup>[15,16]</sup> In contrast, other studies suggested that the primary oxidation onset of PEO-LiTFSI occurs only above 4.6 V versus Li<sup>+</sup>/Li, irrespective of the CAM's structure and chemical composition, or the molecular weight of the PEO used.<sup>[17,18]</sup> To address the obvious inconsistencies in literature regarding the capacity decay of PEO-based SSBs and gain a deeper understanding of the degradation mechanism(s), it is crucial to conduct additional studies on the stability of the PEO-LiTFSI|NCM interface. In fact, in order to enable the commercialization of PEO-based SSBs with Ni-rich cathodes, it is essential to overcome these challenges by developing a full understanding of the degradation mechanisms and developing mitigation strategies.

In this study, we conducted a comprehensive EIS investigation in a three-electrode setup to unequivocally separate the impedance contributions from the cathode and anode side. This allowed us to study the interfacial degradation kinetics and to identify the interface at the cathode side as bottleneck for PEO-based SSBs at high voltages. The results demonstrate that the interfacial stability between NCM and PEO-LiTFSI is influenced by both the applied potential and the molecular weight of the PEO-based SPE. SEM images reveal that the morphology and mechanical properties of PEO change due to the degradation at high potentials, leading to a reduction in viscosity for high molecular weight PEO due to polymer chain cleavage.

## 2. Results and Discussion

The results section of this work is divided into two parts. First, we focus on the electrochemical characterization of the degradation of PEO-based SPEs at various cut-off voltages. In the second part, we shift our attention to the morphological changes of the SPE occurring in the cathode during cycling to different cut-offs.

### 2.1. Electrochemical Investigation of the PEO-LiTFSI|NCM Interface

Electrochemical impedance spectroscopy (EIS) is a non-destructive method to monitor the effects of degradation processes occurring in a battery cell.<sup>[19]</sup> However, the assignment of features in the impedance spectra to single battery cell components can be difficult, since the impedance processes at the anode overlap with the impedance processes at the cathode in PEO-based SSBs, as they occur at similar time constants, as shown by Wurster et al.<sup>[20]</sup> To separate the contributions of the cathode and the anode, we prepared a cell with a  $\mu$ -reference

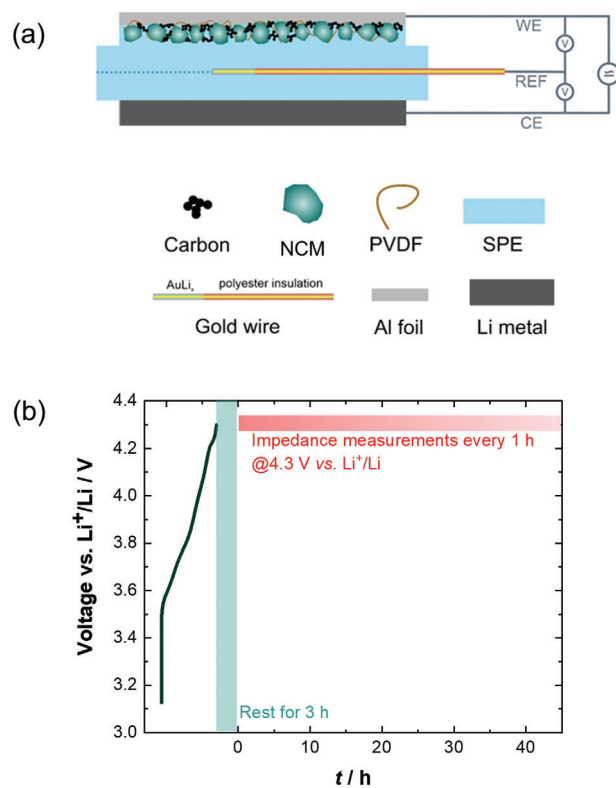


**Figure 1.** a) Schematic of the three-electrode setup to distinguish between the anode and cathode impedance contributions. b) The utilized testing procedure including an initial charge step prior to the constant potential step along with the continuous impedance measurements.

electrode (three-electrode setup (3P)), as shown in **Figure 1a**. The point-like reference electrode was placed centrally between two PEO separators ( $M_w = 8\,000\,000\text{ g mol}^{-1}$ )<sup>[21]</sup> and was lithiated in situ in the fully assembled cell. After the cell was charged to 4.3 V versus Li<sup>+</sup>/Li with a dis-/charge rate of 0.15 C, impedance spectra were collected continuously every hour while holding the potential at 4.3 V versus Li<sup>+</sup>/Li to monitor the impedance growth during the operation and/or storage of batteries in high-voltage conditions (charged state). **Figure 1b** shows a scheme of the measuring procedure used in this study, which is similar to that presented by Kumakura<sup>[22]</sup> from Umicore N.V. at the International Battery Association (IBA) conference in 2022, where the current was measured at different elevated potentials. Nevertheless, to the best of our knowledge the 3P-setup has never been applied to study the impedance in PEO-based SSBs with high-voltage cathodes. The three-electrode cell offers a distinct advantage by allowing the acquisition of not only the whole cell impedance, as achievable with a two-electrode cell, but also enabling the examination of impedance spectra for the individual anode and cathode half-cells.

**Figure 2** illustrates the impedance spectra acquired from the three-electrode cell, showcasing a more comprehensive understanding of the full cell's impedance characteristics. Thereby, the separated cathode and anode half-cell impedance spectra are compared with the spectrum of the full cell after 1 h (**Figure 2a**) and 45 h (**Figure 2b**) at 4.3 V. Interestingly, the cathode and the

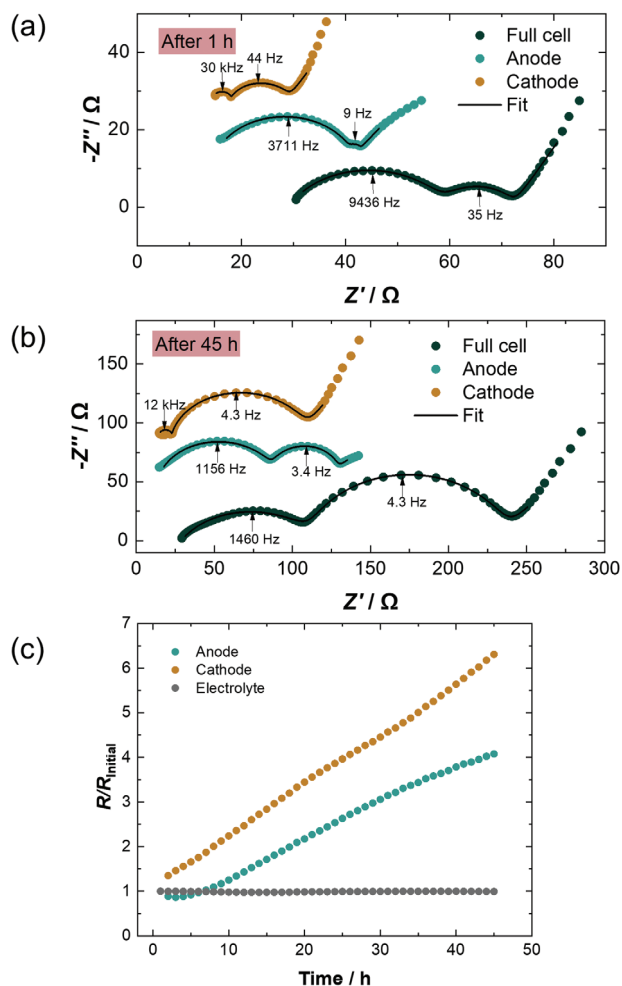


**Figure 2.** Impedance measurements of a 3P-PEO-based SSB with NCM. Impedance spectra of full cell, cathode half-cell, and anode half-cell a) after 1 h and b) after 45 h at 4.3 V versus Li<sup>+</sup>/Li. c) Anode and cathode interface resistance as well as the electrolyte resistance as function of time. Resistances were normalized to their initial values for better comparison. The equivalent circuit is shown in Figure S2 (Supporting Information).

anode half-cell impedance data, as well as the impedance data of the full cell, after 1 h and after 45 h each exhibit two semicircles (the detailed assignment of impedance features to specific physical/electrochemical processes is given below). The analysis of the Distribution of Relaxation Times (DRT) confirms the presence of two main impedance contributions at low and high frequencies (see Figure S1, Supporting Information).

Since the different impedance contributions of anode and cathode have quite close time constants, the differentiation of features from the anode and cathode side from the impedance spectra of cells with only two electrodes is not reliable. Accordingly, a setup with three electrodes is essential and necessary to study the impedance evolution and to understand the reactivity and the degradation kinetics of the individual electrodes. For a quantitative comparison of the impedance contributions, the spectra were fitted using the equivalent circuit shown in Figure S2 (Supporting Information). Subsequently, the total resistance at the cathode and anode side was determined (sum of the two

semicircles) and normalized to the initial impedance after 1 h for better comparability of the impedance evolution. In Figure 2c, we find that the resistance values in the anode and cathode half-cells increase significantly during constant voltage holding, which indicates the occurrence of reactions at the Li|PEO-LiTFSI anode and PEO-LiTFSI|NCM cathode interface. The growth rate of the resistance is significantly higher for the PEO-LiTFSI|NCM interface, which confirms that at high potentials the growth of the cathode impedance is dominating. We note that the increase in impedance at the Li|PEO-LiTFSI interface might also (in part) be related to so-called “cross-talk” phenomena,<sup>[12]</sup> but this is beyond the scope of this study, which focuses on the reactions occurring at the PEO-LiTFSI|NCM interface. However, we refer to extensive work on the Li metal anode interface with PEO electrolytes, in which it was reported, that the middle to high-frequency domain (10<sup>5</sup>–10<sup>2</sup> Hz)<sup>[23]</sup> in the impedance spectra can be attributed to the solid electrolyte interphase (SEI) formed between lithium metal and the SPE, and a lower frequency domain (10<sup>2</sup>–0.1 Hz) corresponds to the charge transfer resistance.<sup>[24]</sup> Both impedance contributions are present in this study. Under static conditions in symmetric Li|SPE|Li cells, a parabolic growth of the SEI between Li and PEO is expected during ageing,<sup>[24]</sup> which is not clearly observed in this study (see Figure 2c). This may be due to the fact of lithium plating (dynamic conditions) before the EIS measurement, as the cells were initially charged to 4.3 V. Accordingly, fresh lithium without native passivation layer<sup>[25]</sup> is deposited on the lithium anode, which is expected to be highly reactive. In this context, it should be noted that the literature on the Li|PEO-LiTFSI interface is often very contradictory. Several authors<sup>[26,24,27,28]</sup> highlighted the instability of this interface. Their results<sup>[29,30]</sup> show that the degradation of the SPE at the lithium anode leads to the formation Li-O-R and LiF compounds. Other studies<sup>[31]</sup> demonstrated that this interfacial degradation is dominated by the reaction of the residual water in the SPE, which leads to the formation of LiOH and Li<sub>2</sub>O. We will follow these interesting anode observations in a forthcoming study applying advanced analytical techniques.

The obtained impedance data confirm that more resistive processes occur at the PEO-LiTFSI|NCM interface. Moreover, the data demonstrate no significant change of the total electrolyte resistance, which was also reported by Li et al.<sup>[32]</sup> (50 cycles with LiCoO<sub>2</sub> as CAM). The obtained values of the bulk resistance correspond approximately to the expected conductivity of PEO-based SPE at 80 °C.

As mentioned above, the impedance spectrum displayed in Figure 2 shows two semicircles for the cathode impedance. According to Illig et al.<sup>[33]</sup> the semicircle at higher frequencies can be assigned to contact resistances between the electrode coating and the current collector, which does not increase significantly after 45 h. However, the low-frequency semicircle, which corresponds to the charge transfer resistance  $R_{CT}$  including the resistance of the cathode electrolyte interphase (CEI)<sup>[20]</sup> is significantly increasing over time  $t$ . In Figure 3, the resistance values for  $R_{CT}$  are plotted over time. The gradual impedance growth confirms that interfacial reactions occur at the PEO-LiTFSI|NCM interface. Interestingly, the growth of the CEI does not follow the Wagner model for diffusion-controlled reactions ( $R_{CT} \sim \sqrt{t}$ ), which was observed, for example, at the interface between sulfide-based SEs and CAMs.<sup>[34]</sup>

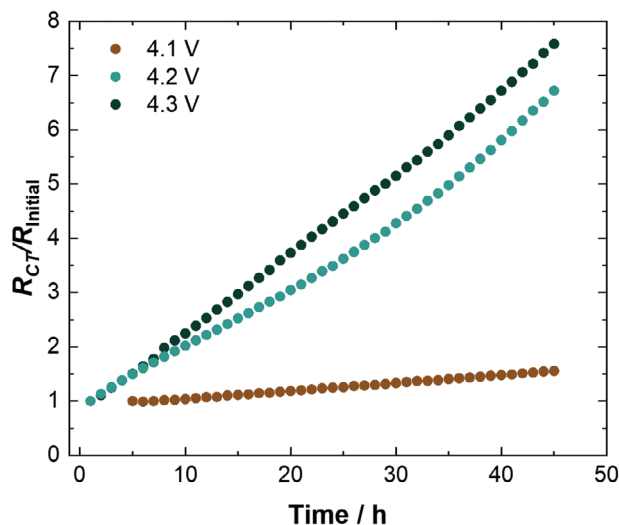


**Figure 3.** Time-dependent changes of the charge transfer resistance  $R_{CT}$  during the constant potential step at 4.1, 4.2, and 4.3 V versus  $\text{Li}^+/\text{Li}$ . The resistances were normalized to their initial values for the sake of comparability.

This rather indicates rate control by the interface reaction itself ( $R_{CT} \sim t$ ).<sup>[35]</sup>

Subsequently, the experiment shown in Figure 1b was repeated applying different cut-off voltages, that is, the PEO-based cells were charged to 4.1 V and to 4.2 V versus  $\text{Li}^+/\text{Li}$ . The corresponding cathode impedance spectra are presented in Figures S3 and S4 (Supporting Information), respectively. The fitted data displayed in Figure 3 show that the impedance growth depends strongly on the cut-off voltage. In fact, the highest increase in resistance after 45 h is observed for the cell charged to 4.3 V cell (by a factor of 7.6) and the lowest for the cell charged to 4.1 V (by a factor of 1.6), indicating a faster and more pronounced growth of the interphase at elevated potentials. Moreover, there is a significant difference between 4.1 and 4.2 V, which indicates some kind of threshold value in this potential range.

To investigate the impact of the interphase growth on the cathode side, as indicated by the EIS data, on the eventual cycling performance, PEO-comprising full cells in a two-electrode setup were subjected to galvanostatic cycling with different upper cut-off voltages (PEO,  $M_w = 8\,000\,000\text{ g mol}^{-1}$ ). Figure 4a displays the charge–discharge curves of the first cycle. No “voltage noise” failure associated with dendrite formation can be seen due to use of higher molecular weight PEO, as shown in our previous study.<sup>[36]</sup>

Please note, that after every charge and discharge step an open-circuit voltage (OCV) step of 2 h was included. The corresponding charge and discharge profiles as function of the cut-off voltage are shown in Figure S5 (Supporting Information). The cells exhibit voltage-dependent charge capacities of  $168\text{ mAh g}^{-1}$  (4.1 V),  $190\text{ mAh g}^{-1}$  (4.2 V), and  $216\text{ mAh g}^{-1}$  (4.3 V). After discharge to 3.0 V, the three cells deliver (reversible) discharge capacities of 158, 181, and  $205\text{ mAh g}^{-1}$ . The higher specific capacity indicates that more lithium can be extracted/intercalated, which depends on the cut-off voltage.

The comparison of the cycling stability (Figure 4b) reveals that the cycling stability is inversely proportional to the applied cut-

off voltage, especially when increasing it to 4.3 V, which is in line with the larger increase of the charge-transfer resistance. In addition, the average voltages during the discharge process were determined (average voltage = total accumulated voltage in a dataset/number of data points). In good agreement with the cycling stability results, the evolution of the overpotential shows a stronger increase for higher cut-off voltages (Figure 4c).

Consequently, the impedance data in a three-electrode setup and the cycling data confirm that the rate of degradation of PEO-based SEs with NCM cathodes is SOC-dependent, suggesting that the electric potential difference between NCM and PEO-LiTFSI at the cathode side is the driving force for the degradation reaction. To investigate the impact of the SPE properties on the stability of PEO-LiTFSI|NCM interface, PEO-based SPEs with different molecular weights were prepared and the same measuring procedure as shown in Figure 1 was conducted. It should be noted that PEO with  $M_w$  of  $8\,000\,000\text{ g mol}^{-1}$  was used as a protective layer for the lithium metal anode in all cells, to prevent dendrite penetration through PEO-based SPE with lower molecular weight that is as shown in previous studies.<sup>[36]</sup> Accordingly, the molecular weight of the SPE was varied only at the cathode side. The corresponding impedance spectra are shown in Figures S6 and S7 (Supporting Information). The corresponding capacities of the interface at the cathode side are illustrated in Figure S8 (Supporting Information) and are in the order of magnitude of literature values.<sup>[37]</sup>

The data in Figure 4d confirm that the growth of the charge transfer resistance is inversely correlated with the molecular weight of PEO-based SPE. As a result, the capacity retention significantly improves with an increase in the molecular weight of PEO during galvanostatic cycling, as illustrated in Figure S9 (Supporting Information). This can be explained by the different concentration of terminal hydroxide groups of PEO-based SPE, which are the limiting factor in the electrochemical stability of PEO-based SPEs according to Yang et al.<sup>[38]</sup> By replacing the  $-\text{OH}$  group with a more stable  $-\text{OCH}_3$  they observed a significant improvement in cycle performance and an extension of the electrochemical stability window from 4.05 to 4.3 V versus  $\text{Li}^+/\text{Li}$ . Accordingly, the concentration of terminal groups is crucial for the growth of charge transfer resistance indicating the growth of a resistive CEI layer. Interestingly, the interfacial degradation kinetics seems to be faster and increasing parabolically, that is, self-accelerating, for lower molecular weight PEO. A parabolic increase of the cathode charge transfer resistance was already observed by Strehle et al.<sup>[39]</sup> with liquid-based electrolytes and NCM. Apparently, the degradation reaction is somehow self-catalyzing, which is of course highly critical. While we consider this observation as highly interesting, the detailed mechanism of this kinetics is beyond the scope of this study and will be subject of future studies. In addition, the conducting salt seems to play a role in the oxidative degradation of the SPE. To ensure comparability to other studies, we focused on a fixed concentration of LiTFSI, which is often used in PEO-based SPEs.<sup>[18,20,24]</sup> However, we intend to vary this parameter systematically in future studies.

Overall, the comprehensive electrochemical investigations provide compelling evidence that the degradation rate of the PEO-LiTFSI|NCM interface is directly influenced by the applied voltage. Notably, within this context, the chemical structure of PEO-based SPEs, especially the concentration of terminal

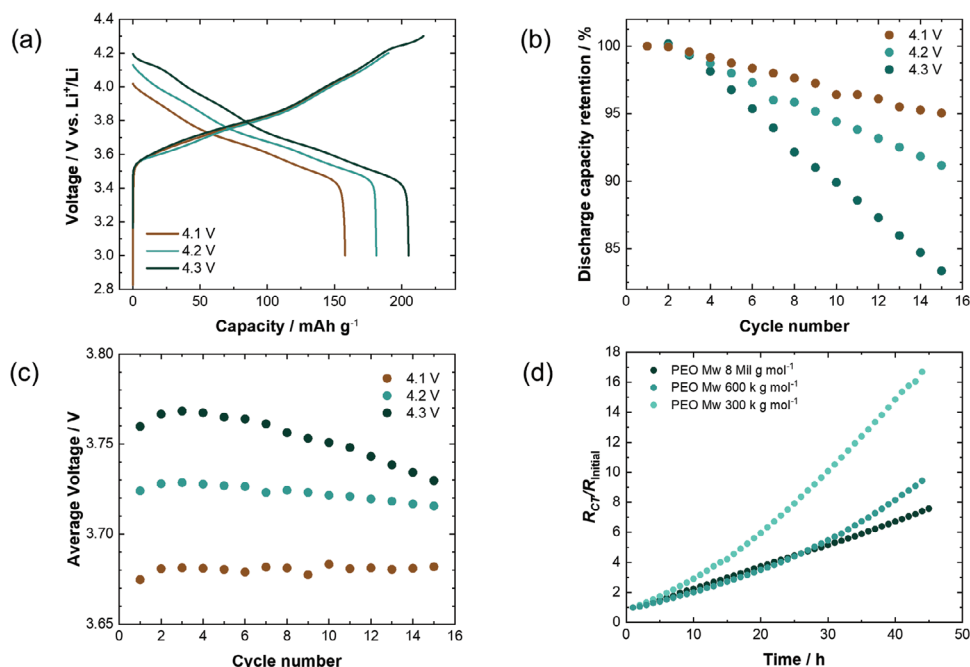


**Figure 4.** Galvanostatic cycling of Li|PEO-LiTFSI|NCM cells applying different upper cut-off voltages: a) charge and discharge curves of the 1st cycle, b) comparison of the capacity retention over 15 cycles, and c) calculated average discharge voltage over 15 cycles. d) Time-dependent changes of the charge transfer resistance  $R_{CT}$  during hold of the potential at 4.3 V of PEO-based SPEs with different molecular weights.

hydroxide groups, seems to be crucial for the interfacial stability and long-term cycle performance with high-voltage cathodes.

## 2.2. Morphological Investigation of the PEO-LiTFSI|NCM Interface

In addition to the electrochemical investigation, the influence of the applied voltage on the cathode morphology related to the oxidative degradation of PEO-based SPEs was examined using scanning electron microscopy (SEM). For this purpose, SEM measurements were conducted after the PEO-based SSBs were cycled with NCM to different cut-off voltages (4 cycles) and compared to open circuit voltage (OCV) conditions, where the cells were stored at the operation temperature (80 °C) but were not cycled. It is important to note that all cells have the same temperature history (storage at 80 °C for 3 days). As demonstrated in Figure 5a,b the cathode morphology of PEO-based SSBs stored at OCV and cycled to 3.6 V versus  $\text{Li}^+/\text{Li}$  are similar. The cathode components seem to be homogeneously distributed, however, large pores are present, since the cathodes were not pressed. In contrast, some of these pores seem to be filled by the SPE after cycling to 4.1 V (Figure 5c) and 4.3 V versus  $\text{Li}^+/\text{Li}$  (Figure 5d). Further SEM images are shown in Figure S10 (Supporting Information). The difference between 4.1 and 4.3 V seem to be not significant. The SEM images indicate that the oxidative degradation of PEO-based SPE during electrochemical cycling to high potentials leads to chain cleavage of the polymer chain. Consequently, shorter polymer chains exhibit lower viscosity, which in our case enables the complete infiltration of the cathode pores with the SPE. With regard to the impedance data in Figure 3 and the gal-

vanostatic cycling data in Figure 4, it seems that the decrease in viscosity that already occurs at 4.1 versus  $\text{Li}^+/\text{Li}$  does not result in a high impedance increase. We conclude that other resistive processes occur at 4.3 V versus  $\text{Li}^+/\text{Li}$  in addition to the mere decrease in SPE viscosity. We like to add that according to the time-of-flight secondary ion mass spectrometry (ToF-SIMS) surface spectra in Figure S11 (Supporting Information), the  $\text{SNO}^-$  and  $\text{C}_2\text{HO}^-$  signals, representing the SPE, are present in all samples at the surface (surface oriented toward the current collector). Accordingly, this indicates that the PEO-based SPE at OCV conditions/cycled to 3.6 V has a sufficiently low viscosity, enabling small amounts of the SPE to infiltrate into the cathode. However, the signal intensity is higher for the cathodes charged to 4.1 and 4.3 V, as shown in Figure S11 (Supporting Information) suggesting a higher fraction of SPE or degraded SPE is present at the surface after cycling to higher potentials, which is consistent with the results from SEM-images. In the corresponding ToF-SIMS spectra, signal intensity of a fragment ( $y$ -axis) is presented as a function of its mass-to-charge ratio ( $x$ -axis).

In addition, focused ion beam (FIB)-SEM measurements under cryogenic conditions were conducted to investigate the cross-section of the cathodes after cycling. For this experiment thicker electrodes were fabricated and pressed before use. As shown in Figure S12 (Supporting Information), while the cathode before cycling shows empty pores, these are filled after cycling to 4.3 V versus  $\text{Li}^+/\text{Li}$  (4 cycles). Overall, these results indicate that electrochemical degradation of the SPE is accompanied by mechanical degradation, leading to a decrease in viscosity. This decrease in viscosity may explain the observed gradual thinning of the SPE during cycling with high voltage cathodes, as degraded PEO with lower viscosity just exits the cell due to the applied

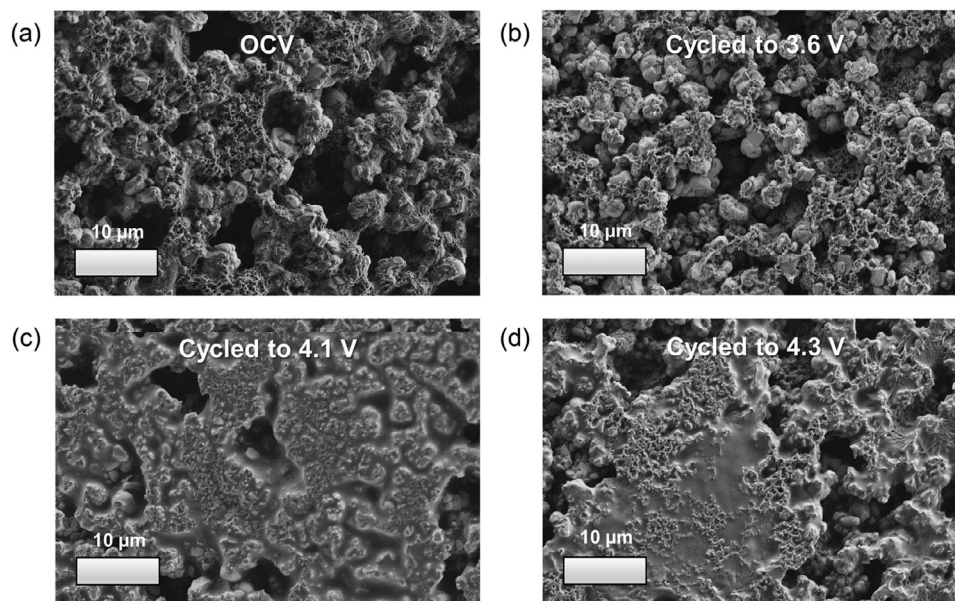


**Figure 5.** SEM images of cathode surfaces oriented toward the current collector after a) OCV conditions and after cycling to b) 3.6 V, c) 4.1 V, and d) 4.3 V versus  $\text{Li}^+/\text{Li}$ .

pressure and/or fills the pores in the cathode, as reported by Kaboli et al.<sup>[11]</sup> The results also support previous studies that have extensively described the chemical degradation mechanism of PEO at high voltages,<sup>[12,13]</sup> attributing the chain cleavage phenomenon to the attack of bis(trifluoromethanesulfonyl)imide acid (HTFSI) on PEO-based SPE. Furthermore, X-ray photoelectron spectroscopy (XPS) has confirmed the formation of ester groups, indicative of oxidized species, in PEO-based SPE after exposure to higher voltages.<sup>[32,40,36]</sup> Based on our findings and the insights presented in existing literature, we believe that the chain cleavage of PEO-SPE stands as a clear marker for the degradation of the SPE. This degradation process is likely a complete decomposition of the polyether structure leading to novel reaction byproducts. Consequently, these can contribute to a notable reduction in ionic conductivity and an increase in charge transfer resistance. This decline is unlikely to be counter-balanced solely by an increase in contact area. As a side note, although the operation temperature (80 °C in this study) is higher than the melting temperature of the SPE ( $\approx 65$  °C), the infiltration of the cathode is determined by the viscosity of the SPE, which is comparably high for PEO with high molecular weight. Further, we like to mention that the contact resistance between the electrode coating and the current collector is apparently not influenced by the infiltration of the SPE into the pores, as the SPE exhibits a negligible electronic conductivity. Accordingly, the size of the semicircle at high frequency in Figure 2 is not changing significantly over time.

While the above summarized results expand our knowledge on the kinetics of PEO degradation at high potentials, there are still many relevant questions that could serve as focal points for future studies. First, the mechanism for the continuous growth of the cathodic charge transfer resistance needs to be further investigated. As suggested above, linear kinetics is typically explained by rate control through an interface reaction. Second, the degradation mechanism of PEO-based SPEs, in particular the

chain cleavage, needs to be confirmed by chemical characterization techniques. Third, since chemical high voltage degradation leads to mechanical degradation of the SPE, the influence of a potential cross-talk (e.g., promoted dendrite formation at the anode side) needs to be clarified by future studies. Based on these investigations, effective protection strategies may be derived as a next step.

### 3. Conclusion

In this study, the interface stability between PEO-based SPE and NCM was re-evaluated, aiming to address inconsistencies in the literature. EIS measurements in a three-electrode setup confirmed that the resistance increase on the cathode side is faster than on the anode side, showing that the PEO/NCM interface is indeed the Achilles' heel in PEO-based SSBs at high voltages. We like to note that also the anode showed a substantial resistance increase, probably related to the reaction between the PEO-SPE and freshly deposited lithium. Moreover, the interfacial stability at the cathode is found to be influenced not only by the cut-off potential but also by the molecular weight of PEO, confirming the crucial role of PEO's terminal groups in the oxidative degradation process of PEO with NCM. These impedance results were supported by galvanostatic cycling data, while SEM images of the cathodes revealed interfacial degradation and polymer chain fragmentation, potentially leading to reduced viscosity. Overall, our findings enhance the understanding of the degradation mechanism involved in PEO-based SSBs with high-voltage cathodes. Future applied research needs to focus on proper protecting coatings on high-voltage cathode materials, like in the case of sulfide-based solid electrolyte. In parallel, improved analytical approaches are needed to acquire true mechanistic information on the PEO|CAM interface reactions.

## 4. Experimental Section

**Materials:** Poly(ethylene oxide) (PEO,  $M_w = 8\,000\,000\text{ g mol}^{-1}$ ,  $M_w = 600\,000\text{ g mol}^{-1}$ , and  $M_w = 300\,000\text{ g mol}^{-1}$ ) and 1-methyl-2-pyrrolidone (NMP, anhydrous, 99.5%) were purchased from Sigma-Aldrich. Lithium bis(trifluoromethanesulfonyl)imide (LiTFSI, 99.9%) and polyvinylidene difluoride (PVDF, Solef 5130) were purchased from Solvay, the conductive carbon (Super P) from Imerys and single crystalline  $\text{LiNi}_{0.83}\text{Co}_{0.11}\text{Mn}_{0.06}\text{O}_2$  were purchased from MSE Supplies. Lithium metal (thickness: 60  $\mu\text{m}$ , Honjo, Japan) was used as counter electrode. The siliconized polyester foil (thickness: 100  $\mu\text{m}$ ) was purchased from Valentia Industries LTD, Ireland, and pouch bag foil from Showa Denko, Japan. All chemicals and cell components were dried under vacuum before use. Material storage, cell assembly, and disassembly for the post-mortem analysis were carried out in an argon-filled glovebox ( $p(\text{H}_2\text{O}, \text{O}_2)/p < 0.1\text{ ppm}$ ).

**PEO Membrane Preparation:** Free-standing PEO-LiTFSI membranes ( $M_w = 300\,000\text{ g mol}^{-1}$ ,  $M_w = 600\,000\text{ g mol}^{-1}$  and  $M_w = 8\,000\,000\text{ g mol}^{-1}$ ) were prepared by a solvent-free technique to exclude any solvent-related influence.<sup>[41]</sup> Therefore, 1000 mg of PEO and 650 mg of LiTFSI (EO/Li ratio 10:1) were intensively mixed until the powders formed a sticky composite. The EO/Li ratio of 10:1 is often used in literature<sup>[20,24,18]</sup> because it enables high ionic conductivity (at elevated temperatures) and appropriate mechanical properties of the SPE. The composite was placed between two siliconized polyester foils, transferred into an aluminum-laminated pouch bag, vacuum sealed (Sealovac) and annealed for 24 h at 90 °C. Subsequently, the pouch bag containing the polymer electrolyte was hot-pressed (Atlas Series Autotouch) between two metal plates at 90 °C and 294 MPa for 15 s. Thus, membranes with a thickness of  $\approx 200\text{--}400\text{ }\mu\text{m}$  were obtained. Finally, the membranes were punched into disks of 12 mm diameter.

**Electrode Preparation and Cell Assembly:** The NCM-based cathodes used in this study consisted of 94 wt.% NCM, 3 wt.% SuperP and 3 wt.% PVDF. Therefore, Super P was homogenized manually in an agate mortar for 5 min and added to a solution of PVDF in NMP. The suspension was mixed for 15 min in a speed mixer (Hauschild DAC 150.1) using  $\text{ZrO}_2$  balls. After adding NCM, the suspension was mixed for another 5 min. The slurries were cast on aluminum foil in argon atmosphere using a doctor blade with a gap of 60  $\mu\text{m}$ , if not specified otherwise. The casting process was followed by drying at 100 °C for 6 h under argon and at 120 °C for 12 h under vacuum. The cathodes were punched into disks of 10 mm diameter and were pressed with 20  $\text{kN cm}^{-2}$ , if not specified otherwise. A cathode thickness of  $\approx 40\text{ }\mu\text{m}$  (including the thickness of the Al sheet,  $\approx 17\text{ }\mu\text{m}$ ) and a porosity of  $\approx 40\%$  were obtained. Pouch bag cells were assembled by subsequently stacking the cathode, one membrane of PEO-LiTFSI (unless otherwise specified) and the lithium metal anode with diameter of 10 mm and were then vacuum sealed (Sealovac). The electrochemical tests were performed at 80 °C using a VMP-300 Biologic potentiostat. The NCM cells were cycled with a dis-/charge rate of 0.15C ( $1\text{C} = 200\text{ mA g}^{-1}$ ).

**EIS (Electrochemical Impedance Spectroscopy):** For the three-electrode setup, a gold wire with a polyester coating (50  $\mu\text{m}$ , GoodFellow) was used, following the approach described by Simon et al.<sup>[42]</sup> To obtain point-like reference electrodes, the polyester was burned at the tip. The obtained micro-reference electrodes were placed in the center of the interface between the two PEO membranes.<sup>[21]</sup> The reference electrodes were lithiated in the fully assembled cell with a constant current of  $-0.5\text{ }\mu\text{A}$  for 12 h at 80 °C (note that the lithiation was only carried out from the lithium side). Using this in situ lithiation process a lithium-gold alloy with a stable potential of 0.30 V versus  $\text{Li}^+/\text{Li}$ <sup>[21,43]</sup> was formed. The cells with the reference electrodes were charged to different potentials versus  $\text{Li}^+/\text{Li}$  using a dis-/charge rate of 0.15 C. The potential was kept constant for 3 h to reach equilibrium prior to the electrochemical impedance spectroscopy (EIS) measurements. This step is necessary to ensure comparability between the samples, since the impedance values of layered cathode oxide materials strongly depend on the lithium content (state of charge) in the cathode.<sup>[44]</sup> The EIS measurements were carried out at 80 °C in a frequency range from 1 to 10 MHz, applying a 20 mV amplitude. The evaluation of the EIS data was performed with the software RelaxIS 3.0.17 (rhd instruments).

**SEM and FIB-SEM:** The morphological characterization was conducted by scanning electron microscopy (SEM) using a Merlin high-resolution scanning electron microscope (Carl Zeiss AG). For the *post mortem* SEM investigation, four types of samples were examined: a cathode from an uncycled cell (after storage at 80 °C) and cathodes from cells, which were cycled with an upper cut-off voltage of 3.6 V, 4.1 and 4.3 V versus  $\text{Li}^+/\text{Li}$  (4 cycles in each case). Due to the sticky properties of the SPE, disassembly of PEO-based cells was experimentally very difficult. Therefore, the cathodes were not pressed/calendared before cell assembly in order to enable the removal of the aluminum current collector after cycling. This allowed to analytically access the PEO/NCM interface. These cathodes had a thickness of  $\approx 45\text{ }\mu\text{m}$  (including the thickness of the Al sheet,  $\approx 17\text{ }\mu\text{m}$ ) and exhibited a comparably high porosity of  $\approx 50\%$ , in contrast to cathodes, that were pressed (porosity of  $\approx 40\%$ ). To ensure comparability, all samples were prepared in the same way having the same temperature history. After the samples were attached to a sample holder using insulating double-sided tape, the samples were transferred from the glovebox to the SEM using an argon-filled LEICA EM VCT500 shuttle (Leica Microsystems) to avoid any contact with the ambient atmosphere.

A focused ion beam (Tescan XEIA3) was used to prepare cross-sections of the pristine and cycled cathodes. For these experiments, thicker cathodes with a wet film thickness of 120  $\mu\text{m}$  were prepared and pressed. The cross-sections were milled with a 2.5  $\mu\text{A}$  Xe-beam under cryo conditions ( $\approx -130\text{ }^\circ\text{C}$ ). The images were taken using an acceleration voltage of 5 kV.

**ToF-SIMS:** Time-of-flight secondary ion mass spectrometry (ToF-SIMS) was performed using an M6 Hybrid SIMS (IONTOF GmbH), which was equipped with a 30 kV Bi-cluster primary ion gun for analysis. The samples were attached to the sample holder using an insulating double-sided tape and were transferred under argon atmosphere from the glovebox to the ToF-SIMS instrument with a LEICA EM VCT500 shuttle (Leica Microsystems). For the surface analysis, the instrument was operated in the spectrometry mode (bunched mode) using  $\text{Bi}_3^+$  ions, which provided high mass resolution (full width at half maximum (FWHM)  $m/\Delta m > 8000$  @  $m/z = 61.97$  (SNO<sup>-</sup>)). The analysis area was set to  $75 \times 75\text{ }\mu\text{m}^2$ , which was rasterized with  $64 \times 64$  pixels and a primary ion dose of  $2.00 \times 10^{12}$  ions  $\text{cm}^{-2}$ . All measurements were carried out in negative ion mode to ensure comparability of the results. The evaluation of the ToF-SIMS data was performed with the software SurfaceLab 7.2 (IONTOF GmbH).

## Supporting Information

Supporting Information is available from the Wiley Online Library or from the author.

## Acknowledgements

The authors would like to acknowledge the financial support from the Federal Ministry of Education and Research (BMBF) within the FestBatt project (03XP0433D and 03XP0429B). D.B. and S.P. would like to thank moreover the Helmholtz Association for the basic funding. A.H. would like to thank the “Professorinnenprogramm III” funded by BMBF, A.H. and J.J. thank the DFG for funding of the Hybrid-SIMS (M6 Hybrid SIMS, IONTOF GmbH, Muenster, Germany) under grant number INST 162/544-1 FUGG.

Open access funding enabled and organized by Projekt DEAL.

## Conflict of Interest

The authors declare no conflict of interest.

## Data Availability Statement

The data that support the findings of this study are available from the corresponding author upon reasonable request.

## Keywords

high-voltage cathode active materials, interface stability, poly(ethylene oxide) (PEO), solid polymer electrolytes, solid-state batteries

Received: June 21, 2023  
Revised: October 15, 2023  
Published online:

- [1] J. Janek, W. G. Zeier, *Nat. Energy* **2016**, *1*, 16141.  
[2] Y.-K. Sun, *ACS Energy Lett.* **2020**, *5*, 3221.  
[3] Z. Gao, H. Sun, L. Fu, F. Ye, Y. Zhang, W. Luo, Y. Huang, *Adv. Mater.* **2018**, *30*, 1870122.  
[4] R. C. Agrawal, G. P. Pandey, *J. Phys. D: Appl. Phys.* **2008**, *41*, 223001.  
[5] M. Shoji, E. J. Cheng, T. Kimura, K. Kanamura, *J. Phys. D: Appl. Phys.* **2019**, *52*, 103001.  
[6] J. Liang, X. Li, S. Wang, K. R. Adair, W. Li, Y. Zhao, C. Wang, Y. Hu, L. Zhang, S. Zhao, S. Lu, H. Huang, R. Li, Y. Mo, X. Sun, *J. Am. Chem. Soc.* **2020**, *142*, 7012.  
[7] G. B. Appetecchi, F. Alessandrini, R. G. Duan, A. Arzu, S. Passerini, *J. Power Sources* **2001**, *101*, 42.  
[8] A. Gupta, J. Sakamoto, *Electrochem. Soc. Interface* **2019**, *28*, 63.  
[9] L. Xu, J. Li, W. Deng, L. Li, G. Zou, H. Hou, L. Huang, X. Ji, *Mater. Chem. Front.* **2021**, *5*, 1315.  
[10] J. Liang, Y. Sun, Y. Zhao, Q. Sun, J. Luo, F. Zhao, X. Lin, X. Li, R. Li, L. Zhang, S. Lu, H. Huang, X. Sun, *J. Mater. Chem. A* **2020**, *8*, 2769.  
[11] S. Kaboli, H. Demers, A. Paolella, A. Darwiche, M. Dontigny, D. Clément, A. Guerfi, M. L. Trudeau, J. B. Goodenough, K. Zaghib, *Nano Lett.* **2020**, *20*, 1607.  
[12] K. Nie, X. Wang, J. Qiu, Y. Wang, Q. Yang, J. Xu, X. Yu, H. Li, X. Huang, L. Chen, *ACS Energy Lett.* **2020**, *5*, 826.  
[13] L. Seidl, R. Grissa, L. Zhang, S. Trabesinger, C. Battaglia, *Adv. Mater. Interfaces* **2022**, *9*, 2100704.  
[14] J. Ma, Z. Liu, B. Chen, L. Wang, L. Yue, H. Liu, J. Zhang, Z. Liu, G. Cui, *J. Electrochem. Soc.* **2017**, *164*, A3454.  
[15] J. Qiu, X. Liu, R. Chen, Q. Li, Y. Wang, P. Chen, L. Gan, S.-J. Lee, D. Nordlund, Y. Liu, X. Yu, X. Bai, H. Li, L. Chen, *Adv. Funct. Mater.* **2020**, *30*, 1909392.  
[16] J. Liang, S. Hwang, S. Li, J. Luo, Y. Sun, Y. Zhao, Q. Sun, W. Li, M. Li, M. N. Banis, X. Li, R. Li, L. Zhang, S. Zhao, S. Lu, H. Huang, D. Su, X. Sun, *Nano Energy* **2020**, *78*, 105107.  
[17] G. Homann, L. Stolz, J. Nair, I. C. Laskovic, M. Winter, J. Kasnatscheew, *Sci. Rep.* **2020**, *10*, 4390.  
[18] G. Homann, L. Stolz, K. Neuhaus, M. Winter, J. Kasnatscheew, *Adv. Funct. Mater.* **2020**, *30*, 2006289.  
[19] L. A. Middlemiss, A. J. R. Rennie, R. Sayers, A. R. West, *Energy Rep.* **2020**, *6*, 232.  
[20] V. Wurster, C. Engel, H. Graebe, T. Ferber, W. Jaegermann, R. Hausbrand, *J. Electrochem. Soc.* **2019**, *166*, A5410.  
[21] J. Landesfeind, D. Pritzl, H. A. Gasteiger, *J. Electrochem. Soc.* **2017**, *164*, A1773.  
[22] S. Kumakura from Umicore, "Strategy to Optimize Nmc Materials for All-Solid State Batteries", Presentation at International Battery Association October 4, 2022 Bled, Slovenia.  
[23] R. Bouchet, S. Lascaud, M. Rosso, *J. Electrochem. Soc.* **2003**, *150*, A1385.  
[24] F. J. Simon, M. Hanauer, F. H. Richter, J. Janek, *ACS Appl. Mater. Interfaces* **2020**, *12*, 11713.  
[25] S.-K. Otto, Y. Moryson, T. Krauskopf, K. Peppler, J. Sann, J. Janek, A. Henss, *Chem. Mater.* **2021**, *33*, 859.  
[26] H. Liang, S. Wang, Q. Ye, C. Zeng, Z. Tong, Y. Ma, H. Li, *Chem. Commun.* **2022**, *58*, 10821.  
[27] E. E. Ushakova, A. Frolov, A. A. Reveguk, D. Y. Usachov, D. M. Itkis, L. V. Yashina, *Appl. Surf. Sci.* **2022**, *589*, 153014.  
[28] O. Sheng, J. Zheng, Z. Ju, C. Jin, Y. Wang, M. Chen, J. Nai, T. Liu, W. Zhang, Y. Liu, X. Tao, *Adv. Mater.* **2020**, *32*, 2000223.  
[29] M. Le Granvalet-Mancini, *Solid State Ionics* **2000**, *135*, 283.  
[30] E. K. W. Andersson, C. Sängeland, E. Berggren, F. O. L. Johansson, D. Kühn, A. Lindblad, J. Mindemark, M. Hahlin, *J. Mater. Chem. A* **2021**, *9*, 22462.  
[31] H. Cheng, C. B. Zhu, M. Lu, Y. Yang, *J. Power Sources* **2007**, *174*, 1027.  
[32] J. Li, Y. Ji, H. Song, S. Chen, S. Ding, B. Zhang, L. Yang, Y. Song, F. Pan, *Nano-Micro Lett.* **2022**, *14*, 191.  
[33] J. Illig, J. P. Schmidt, M. Weiss, A. Weber, E. Ivers-Tiffée, *J. Power Sources* **2013**, *239*, 670.  
[34] T.-T. Zuo, R. Rueß, R. Pan, F. Walther, M. Rohnke, S. Hori, R. Kanno, D. Schröder, J. Janek, *Nat. Commun.* **2021**, *12*, 6669.  
[35] H. Schmalzried, *Chemical Kinetics of Solids*, Wiley-VCH, Weinheim **1995**.  
[36] Y. Yusim, E. Trevisanello, R. Ruess, F. H. Richter, A. Mayer, D. Bresser, S. Passerini, J. Janek, A. Henss, *Angew. Chem., Int. Ed.* **2023**, *62*, e202218316.  
[37] E. Trevisanello, R. Ruess, G. Conforto, F. H. Richter, J. Janek, *Adv. Energy Mater.* **2021**, *11*, 2003400.  
[38] X. Yang, M. Jiang, X. Gao, D. Bao, Q. Sun, N. Holmes, H. Duan, S. Mukherjee, K. Adair, C. Zhao, J. Liang, W. Li, J. Li, Y. Liu, H. Huang, L. Zhang, S. Lu, Q. Lu, R. Li, C. V. Singh, X. Sun, *Energy Environ. Sci.* **2020**, *13*, 1318.  
[39] B. Strehle, F. Friedrich, H. A. Gasteiger, *J. Electrochem. Soc.* **2021**, *168*, 050512.  
[40] J. Liang, D. Chen, K. Adair, Q. Sun, N. G. Holmes, Y. Zhao, Y. Sun, J. Luo, R. Li, L. Zhang, S. Zhao, S. Lu, H. Huang, X. Zhang, C. V. Singh, X. Sun, *Adv. Energy Mater.* **2021**, *11*, 2002455.  
[41] G. B. Appetecchi, M. Carewska, F. Alessandrini, P. P. Prosini, S. Passerini, *J. Electrochem. Soc.* **2000**, *147*, 451.  
[42] F. J. Simon, L. Blume, M. Hanauer, U. Sauter, J. Janek, *J. Electrochem. Soc.* **2018**, *165*, A1363.  
[43] S. Solchenbach, D. Pritzl, E. J. Y. Kong, J. Landesfeind, H. A. Gasteiger, *J. Electrochem. Soc.* **2016**, *163*, A2265.  
[44] <number>[44]</number>R. S. Negi, P. Minnmann, R. Pan, S. Ahmed, M. J. Herzog, K. Volz, R. Takata, F. Schmidt, J. Janek, M. T. Elm, *Chem. Mater.* **2021**, *33*, 6713.